

Physical Simulation of Moisture Induced Thin Shell Deformation

ANONYMOUS AUTHOR(S)

ACM Reference Format:

Anonymous Author(s). 2018. Physical Simulation of Moisture Induced Thin Shell Deformation. 1, 1 (December 2018), 8 pages. <https://doi.org/10.1145/888888.777777>

1 INTRODUCTION

Contribution. We present a low-order discrete shell model tailored to simulating non-uniform, anisotropic, differential swelling and shrinking of thin shells. In contrast to previous methods for simulating related phenomena, such as burning and growth, our formulation builds on discrete geometric shell theory and supports arbitrary rest curvature and strain, and physical settings such as thickness and Lamé parameters. We couple our shell model to a simple formulation of moisture diffusion in both the lateral and thickness directions, which takes into account anisotropy of the material grain. In a series of experiments, we show that our model successfully predicts the qualitative behavior of thin shells undergoing complex, dynamic deformations due to swelling or shrinking, such as occurs when paper is moistened, leaves dry in the sun, or thin plastic melts.

1.1 Related Work

Simulating Burning/Melting/Swelling. Several papers look at related problems, such as evolving the boundary of a burning or melting solid, without incorporating curling/wrinkling and other elastic deformations of the solid. Melek and Keyser [2003; 2005] simulate pyrolysis and heat diffusion of burning objects, but do not consider elastic deformation of the burning objects. Losasso et al [2006] proposed tracking of the burning boundary of thin shells using an adaptive level set on the shell. Some of the deformation can be qualitatively approximated by mapping physical quantities like heat and moisture to cells of a coarse grid around the object, deforming the cage, and mapping the deformation back onto the shell (as in Free Form Deformation); this approach was proposed by Melek and Keyser [2007] and adopted by Liu et al [2009]. Most similar to our work is the method of Jeong et al [2011; 2013], which uses a *bilayer* of springs (a triangle mesh and its circumcentric dual, offset a distance from the primal mesh) to represent the shell. The bilayer allows the method to capture *differential* growth due to gradients in moisture concentration across the thickness of leaves, leading to visually impressive simulations of leaves curling as they dry. Our work is based on the same fundamental idea (representing the shell using rest geometry that varies linearly through the thickness) but couched in the machinery of differential geometry; our formulation

Permission to make digital or hard copies of part or all of this work for personal or classroom use is granted without fee provided that copies are not made or distributed for profit or commercial advantage and that copies bear this notice and the full citation on the first page. Copyrights for third-party components of this work must be honored. For all other uses, contact the owner/author(s).

© 2018 Copyright held by the owner/author(s).
XXXX-XXXX/2018/12-ART
<https://doi.org/10.1145/888888.777777>

allows us to easily incorporate non-zero rest curvature, machine direction, and a physical material model.

Steps towards a principled physical model include the use of a mass-spring network to represent the shell, with update rules for how spring rest lengths should change due to physical processes in the shell. Such rules are simplest to formulate in the case where growth or shrinkage is uniform through the shell thickness, and the shell can be represented using a single spring layer; Larboulette et al [2013] present such a rule, which includes handling of the *machine direction* of paper: a bias in the orientation of the fibers composing the paper which causes the paper to swell anisotropically. We adopt this parameter in our material model.

Mechanics of Shells. The mathematics and geometry underpinning the physics of thin shells is a venerable topic: Ciarlet's book [2000] on elasticity as applied to shells offers a thorough overview. Our work is based on the common *Kirchhoff-Love* assumption that the shell does not undergo any transverse shear; ie, that the shell volume is foliated by normal offsets of the shell's *midsurface*: the problem of studying deformation of the 3D shell volume then reduces to that of deformation of a 2D surface, and tools from Riemannian geometry can be applied [Simo and Fox 1989]. (We adopt the so-called "intrinsic" view [Neff 2004] that shells can be understood in terms of Kirchhoff-Love and geometric principles, as this view allows us to easily discretize shell physics by leveraging discrete differential geometry, but we note in passing that the validity of the Kirchhoff-Love assumption, and of reduced shell models in general, remains unsettled, and the literature documents numerous alternative shell theories.) One key property of the shells we want to simulate is that they are *non-Euclidean*: they do not have a rest (strain-free) state that is realizable in three-dimensional space. Non-Euclidean shells have received substantial attention recently in the physics community [Kim et al. 2012; Klein et al. 2007], thanks to their potential applications in fabrication and robotics, and their connection to biological growth; Sharon and Efrati [Efrati et al. 2009; Sharon and Efrati 2010] pioneered the study of shell mechanics in this setting.

For the sake of being self-contained, we briefly review the geometric foundations of shell mechanics in Section 2.

Computational Modeling of Thin Shells. Thin shells first caught the interest of the graphics community in the context of simulating cloth [Baraff and Witkin 1998; Bridson et al. 2002]. These early methods tended to focus on thin *plates*, i.e. shells that are rest flat, and formulate shell dynamics either in terms of either hinge-based bending energies [Sullivan 2008; Tamstorf and Grinspun 2013] or the insight that the bending energy can be written in terms of the intrinsic Laplace-Beltrami operator applied to the shell's embedding function [Bergou et al. 2006; Bobenko and Schröder 2005; Wardetzky et al. 2007]. Grinspun et al [2003] introduced to graphics the simulation of shells with non-flat rest curvature. Their formulation is based on *differences of squared mean curvature*, leading to a simple

and easy-to-discrete bending energy; this model is physically suspect, however: consider a half-cylinder at rest when curled around the x -axis. Unbend the shell and re-bend it around the y -axis; the deformed configuration's strain cannot be captured by looking at mean curvature alone, as it is pointwise identical to the mean curvature of the rest configuration. Complete support for rest curvature requires a bending energy that incorporates full information about the extrinsic deformation of the shell [Grinspun et al. 2006]. One recent such discrete energy is described in Weischedel's under-appreciated work on discrete Cosserat shells [2012]; our exposition is modeled closely on hers, though we make different modeling choices (we use an intrinsic rather than Cosserat shell model, and require more flexible handling of the shell rest geometry).

Higher-order methods for simulating shells (including with e.g. NURBS or subdivision elements) are common in computational mechanics and isogeometric analysis [Bandara and Cirak 2018; Bathe et al. 1983; Batoz et al. 1980; Benson et al. 2010; Cirak et al. 2000; Kiendl et al. 2009] and have also been proposed for computer graphics [Wawrzinek et al. 2011]. High-order methods have some obvious advantages (better convergence behavior in the thin limit, especially for shell deformations involving large strains; continuous surface normals) at the cost of additional computational cost and complexity, especially when handling contact.

In this paper, we ignore the problem of mesh tesselation, or of adapting the mesh in response to either large deflections or large amounts of growth; such remeshing is an important component of a practical shell simulation but orthogonal to our focus on shell dynamics. ArcSim [Narain et al. 2012] incorporates a method of adaptive remeshing while avoiding significant popping artifacts, and has been used to generate impressive simulations of creasing paper. Vetter et al [2013] study the companion problem of remeshing due to large in-plane growth, and present a solution based on adaptive Loop subdivision.

2 CONTINUOUS FORMULATION

Before describing our discretization of shells, we briefly review the formulation in the continuous setting, as this formulation will guide our discretization.

Shell Geometry. We can represent shells $S \subset \mathbb{R}^3$ of thickness h by a parameter domain Ω in the plane and an embedding $\phi : \Omega \times [-h/2, h/2] \rightarrow \mathbb{R}^3$ with S the image of ϕ (see Figure ??). We adopt the common Kirchhoff-Love assumption that the shell does not undergo any transverse shear; ie, that the shell volume is foliated by normal offsets of the shell's *midsurface* $\mathbf{r} : \Omega \rightarrow \mathbb{R}^3$. In other words,

$$\phi(x, y, z) = \mathbf{r}(x, y) + z\hat{\mathbf{n}}(x, y)$$

where $\hat{\mathbf{n}} = (\mathbf{r}_x \times \mathbf{r}_y) / \|\mathbf{r}_x \times \mathbf{r}_y\|$ is the midsurface normal. The shell's deformation is thus completely determined by the deformation of the midsurface. The metric g on the slab $\Omega \times [-h/2, h/2]$, pulled back from \mathbb{R}^3 , can be expressed in terms of the geometry of the midsurface:

$$g = \begin{bmatrix} a - 2zb + z^2c & 0 \\ 0 & 1 \end{bmatrix}, \quad (1)$$

where

$$\mathbf{a} = d\mathbf{r}^T d\mathbf{r} \quad \mathbf{b} = -d\mathbf{r}^T d\hat{\mathbf{n}} \quad \mathbf{c} = d\hat{\mathbf{n}}^T d\hat{\mathbf{n}}$$

are the classical first, second, and third fundamental forms of the surface \mathbf{r} .

Oftentimes, the parameterization domain of a thin shell is assumed to be also the rest state of the shell, so that the strain in the material of the shell can be determined directly from looking at g . We cannot assume this: consider for instance a piece of paper whose center has been moistened by spilled coffee. The fibers in the coffee stain stretch; since they are confined by the surrounding non-wet region of the paper, the paper cannot globally stretch in such a way that both the wet and dry regions of the paper are simultaneously at rest. Instead, the paper will *buckle* out of plane, into a shape that compromises between relaxing the in-plane (stretching) strain and the introduced bending strain. At this point the paper's rest state is *non-Euclidean*—it is impossible to find any embedding of the paper into \mathbb{R}^3 that is entirely strain-free.

We therefore record the rest state of the shell using a *rest metric* $\bar{g}(x, y, z)$.¹ Since our model is tailored to simulating differential in-plane swelling or shrinking across the thickness of the shell, we make the simplifying assumption that this rest metric is linear in the thickness direction, and does not affect the shell thickness:

$$\bar{g}(x, y, z) = \bar{\mathbf{a}}(x, y) - 2z\bar{\mathbf{b}}(x, y).$$

A shell that begins a simulation at rest will simply have $\bar{\mathbf{a}} = \mathbf{a}$ and $\bar{\mathbf{b}} = \mathbf{b}$; similarly, in the case that the shell *does* have a rest state $\bar{\mathbf{r}}$ that is isometrically embeddable in \mathbb{R}^3 , a and b are the first and second fundamental forms of the surface $\bar{\mathbf{r}}$. Therefore \mathbf{a} and \mathbf{b} can be thought of as representing the “rest metric” and “rest curvature” of the shell, respectively.²

Finally, we cannot assume that the shell has uniform density, since different parts of the shell might gain or lose mass due to absorbing or releasing moisture. We therefore allow the density per unit *rest* volume $\rho(x, y)$ to vary over Ω . (In principle, we could also model the variation in density across the shell thickness; however doing so leads only to a small ($O(h^3)$) correction to the shell's kinetic energy, and since the swelling phenomena we are interested in simulating tend to happen over relatively long time scales, there is no need for such accuracy.)

To summarize, our parameterization of thin shells involves the following kinematic elements:

- a thickness h and parameterization domain $\Omega \subset \mathbb{R}^2$, both of which are fixed over the course of the simulation;
- an embedding $\mathbf{r} : \Omega \rightarrow \mathbb{R}^3$ representing the shell midsurface's “current”/“deformed” geometry, and which evolves over time. From this midsurface embedding, the embedding of the full shell volume ϕ , and the midsurface fundamental forms, can be calculated;
- a rest metric and density, parameterized by the pair of tensor field $\bar{\mathbf{a}}, \bar{\mathbf{b}}$ and a scalar field ρ over Ω , respectively. These might also evolve over time, due to changes in the shell rest state via growth or shrinkage.

¹Here and throughout the paper, we use an overbar to denote quantities associated to the shell rest state.

²We stress, though, that these labels are to provide intuition only— $\bar{\mathbf{a}}$ and $\bar{\mathbf{b}}$ must not, and generally will not, satisfy usual relationships from differential geometry such as the Gauss-Codazzi-Mainardi equations.

2.1 Shell Dynamics

Motivated by the common observation that a sufficiently thin shell bends much more readily than it will stretch, we assume that the shell's deformation involves *large rotations* but only small in-plane strain of the midsurface: $\|\bar{\mathbf{a}}^{-1}\mathbf{a} - \mathbf{I}\|_\infty < h$. We also assume that the shell's material is uniform and isotropic. The simplest constitutive law consistent with these assumptions is to use a St. Venant-Kirchhoff material model³ together with Green strain; it can be shown [?] that these choices yield an elastic energy density (the *Koiter shell model*) that can be approximated up to $O(h^4)$ by

$$W(x, y) = \left(\frac{h}{4} \|\bar{\mathbf{a}}^{-1}\mathbf{a} - \mathbf{I}\|_{SV}^2 + \frac{h^3}{12} \|\bar{\mathbf{a}}^{-1}(\mathbf{b} - \bar{\mathbf{b}})\|_{SV}^2 \right) \sqrt{\det \bar{\mathbf{a}}} \quad (2)$$

where $\|\cdot\|_{SV}$ is the "St. Venant-Kirchhoff norm" [Weischedel 2012]

$$\|M\|_{SV} = \frac{\alpha}{2} \operatorname{tr}^2 M + \beta \operatorname{tr}(M^2),$$

for Lamé parameters α, β . In terms of the Young's modulus E and Poisson's ratio ν ,

$$\alpha = \frac{Ev}{(1+\nu)(1-2\nu)}, \quad \beta = \frac{E}{2(1+\nu)}.$$

We thus have a formulation of kinetic energy and potential energy

$$T[\mathbf{f}] = \int_{\Omega} h\rho \|\dot{\mathbf{r}}\|^2 \sqrt{\det \bar{\mathbf{a}}} dx dy, \quad V[\mathbf{r}] = \int_{\Omega} W(x, y) dx dy,$$

to which additional external energies and forces (gravity, constraint forces, etc) can be added to yield equations of motion via the usual principle of least action.

3 DISCRETIZATION

We approximate the midsurface \mathbf{r} with a triangle mesh (V, E, F) ; the positions of the vertices $\mathbf{v} = [\mathbf{v}_1, \mathbf{v}_2 \dots]$ take the place of the embedding function \mathbf{r} . The general strategy we will use is to assume that \mathbf{a} and \mathbf{b} , as well as their rest counterparts $\bar{\mathbf{a}}$ and $\bar{\mathbf{b}}$, are constant over each face of a triangle mesh representing the shell midsurface; it will then be relatively straightforward to write down a discrete analogue of the Koiter elastic energy density in Equation (2).

Discrete Shell Model. As in the continuous setting, the discrete shell does not necessarily have a rest state embeddable as a mesh in \mathbb{R}^3 , making it impossible to parameterize the deformed configuration of the shell in terms of the rest configuration; additionally we do not want to assume (or compute) a global parameterization of the midsurface. Instead, we independently parameterize each triangle in its own barycentric coordinates (see Figure ??). Let \mathbf{f}_{ijk} be a face in F containing the vertices $\mathbf{v}_i, \mathbf{v}_j, \mathbf{v}_k$, and denote by \mathcal{T} the canonical unit triangle with vertices $(0, 0), (1, 0), (0, 1)$. Then locally the face \mathbf{f}_{ijk} is embedded by the affine function

$$\mathbf{r}_{ijk} : \mathcal{T} \rightarrow \mathbb{R}^3, \quad \mathbf{r}_{ijk}(u_1, u_2) = \mathbf{v}_i + u_1(\mathbf{v}_j - \mathbf{v}_i) + u_2(\mathbf{v}_k - \mathbf{v}_i);$$

under this embedding, the Euclidean metric on face \mathbf{f}_{ijk} pulls back to the constant first fundamental form

$$\mathbf{a}_{ijk} = \begin{bmatrix} \|\mathbf{v}_j - \mathbf{v}_i\|^2 & (\mathbf{v}_j - \mathbf{v}_i) \cdot (\mathbf{v}_k - \mathbf{v}_i) \\ (\mathbf{v}_j - \mathbf{v}_i) \cdot (\mathbf{v}_k - \mathbf{v}_i) & \|\mathbf{v}_k - \mathbf{v}_i\|^2 \end{bmatrix}$$

³The neo-Hookean material model is also popular in computer graphics and could be used instead, although there is little benefit to doing so when simulating thin shells since strains are typically small.

on \mathcal{T} . If we are given an explicit rest configuration $\bar{\mathbf{v}}_i$ of the shell, we can compute the rest first fundamental form $\bar{\mathbf{a}}_{ijk}$ analogously; or alternatively we can set $\bar{\mathbf{a}}_{ijk}$ to any desired symmetric positive-definite 2×2 matrix. Notice that any such matrix corresponds to some choice of "rest lengths" for the edges of face \mathbf{f}_{ijk} that obey the triangle inequality, but that two faces sharing a common edge do not necessarily agree about that length.

These discrete fundamental forms are enough to discretize the stretching term in Equation (2): each face contributes a term

$$\begin{aligned} & \int_{\mathcal{T}} \frac{h}{4} \|\bar{\mathbf{a}}_{ijk}^{-1} \mathbf{a}_{ijk} - \mathbf{I}\|_{SV}^2 \sqrt{\det \bar{\mathbf{a}}_{ijk}} \\ &= \frac{h}{8} \|\bar{\mathbf{a}}_{ijk}^{-1} \mathbf{a}_{ijk} - \mathbf{I}\|_{SV}^2 \sqrt{\det \bar{\mathbf{a}}_{ijk}}. \end{aligned}$$

This energy is quartic in the positions of the mesh vertices, and is exactly the energy of constant-strain triangle stretching elements commonly used in cloth simulation.

For the bending term, we also need a discretization of the second fundamental form. Here there is a significant departure between the smooth theory and the discrete approximation: we would like to apply the Kirchhoff-Love principle to extrude the mid-surface into a shell volume, but unfortunately distance offsets of triangle meshes are no longer guaranteed to be triangle meshes (or even piecewise-affine). One can instead look at weaker notions of mesh parallelity [Bobenko et al. 2010]:

- *vertex offsets* require choosing a normal at each mesh vertex (itself a problem without an obvious solution), and moving each vertex a constant distance along this normal usually does not result in faces parallel to the original faces;
- *edge offsets* likewise do not guarantee parallel faces;
- *face offsets* are not conforming: moving each face around a vertex of valence four or higher in their normal direction yields new faces that are not guaranteed to still intersect at a common point.

We use the discretization that arises from edge parallelity, leading to the so-called "mid-edge" discretization of the second fundamental form [Grinspun et al. 2006; Weischedel 2012]: let \mathbf{e}_i denote the edge opposite vertex i on face \mathbf{f}_{ijk} , and define the *mid-edge normal* $\hat{\mathbf{n}}_i$ by:

- the face normal $\frac{(\mathbf{v}_j - \mathbf{v}_i) \times (\mathbf{v}_k - \mathbf{v}_i)}{\|(\mathbf{v}_j - \mathbf{v}_i) \times (\mathbf{v}_k - \mathbf{v}_i)\|}$, if \mathbf{e}_i is a boundary edge;
- the mean of the face normals of the two faces incident on \mathbf{e}_i , otherwise.

Let $\mathbf{f}_{ijk}^\epsilon$ denote the triangle formed by offsetting all of \mathbf{f}_{ijk} 's edges in their mid-edge normal direction by a distance ϵ , and let $\mathbf{a}_{ijk}^\epsilon$ be the discrete first fundamental form of that offset triangle. Then the discrete second fundamental form \mathbf{b} can be defined, by analogy to Equation (1), as the first-order correction

$$\mathbf{a}_{ijk}^\epsilon = \mathbf{a}_{ijk} - 2\epsilon \mathbf{b}_{ijk} + O(\epsilon^2),$$

leading to the formula

$$\mathbf{b}_{ijk} = \frac{1}{2} \begin{bmatrix} (\hat{\mathbf{n}}_i - \hat{\mathbf{n}}_j) \cdot (\mathbf{v}_i - \mathbf{v}_j) & (\hat{\mathbf{n}}_i - \hat{\mathbf{n}}_j) \cdot (\mathbf{v}_i - \mathbf{v}_k) \\ (\hat{\mathbf{n}}_i - \hat{\mathbf{n}}_k) \cdot (\mathbf{v}_i - \mathbf{v}_j) & (\hat{\mathbf{n}}_i - \hat{\mathbf{n}}_k) \cdot (\mathbf{v}_i - \mathbf{v}_k) \end{bmatrix}.$$

(Alternatively, this formula can be derived by discretizing the relation $\mathbf{b} = -d\mathbf{r}^T d\hat{\mathbf{n}}$ using divided differences). Although it may not appear so at first, the matrix \mathbf{b}_{ijk} is always symmetric (since each

mid-edge normal is orthogonal to that edge); it is not in general positive-definite.⁴ We represent the rest second fundamental form \bar{b}_{ijk} by an arbitrary symmetric 2×2 matrix assigned to each face.

Choosing Rest Fundamental Forms. Depending on the mechanism for growth being simulated, there are several choices for how to set and update \bar{a} and \bar{b} :

- **No Growth:** A classic shell, whose rest state is fixed, simply has $\bar{a} = a^0$ and $\bar{b} = b^0$, where a^0 denotes the first fundamental form induced by v^0 , the positions of the midsurface vertices at the beginning of the simulation. (And if the shell is pre-stressed, \bar{a}, \bar{b} can be adjusted appropriately).
- **Pullback Forms:** In the case where the shell's initial configuration is flat, it is natural to align it with a region of the xy plane, and prescribe rest fundamental forms on $\text{im } r$ in Euclidean x, y coordinates. Let \bar{a}^{xy} and \bar{b}^{xy} be such prescribed forms; these can be sampled per triangle $f_{i,j,k}$ and pulled back to the triangle's parameterization domain to give

$$\bar{a} = T^T \bar{a}^{xy}(c)T, \quad T^T \bar{b}^{xy}(c)T,$$

where

$$T = \begin{bmatrix} v_j^0 - v_i^0 & v_k^0 - v_i^0 \end{bmatrix}$$

maps from vectors in the barycentric coordinates of f_{ijk} to Euclidean space, and $c = \frac{1}{3}(v_i + v_j + v_k)$ is the face centroid.

- **Isotropic Growth:** In many cases growth is isotropic and uniform through the thickness of the shell (for instance, when plastic shrinks in response to heat, or plant tissue grows through cell division). In this case

$$\bar{a} = e^{2s_{ijk}} a^0, \quad \bar{b} = b^0$$

for a conformal factor s encoding the amount of growth (or shrinking, if negative).

- **Linear Differential Swelling:** Porous materials like paper swell when moistened, and differences in water concentration through the thickness of a thin shell can induce metric frustration and buckling. This mechanism is responsible for the buckling of paper when wet, and the curling of leaves as they dry.

We model this swelling mechanism by assuming that the amount of moisture varies linearly in the thickness direction of the shell, and present the percentage of additional moisture present in the material at the top and bottom of the shell by two scalars $m_{ijk}^+, m_{ijk}^- \in \mathbb{R}$. For example, complete dessication of the top of the shell, and doubling of the moisture content at the bottom, would be presented by values $m^+ = -100, m^- = 100$. The additional water content induces swelling, which changes the rest geometry; assuming a linear relationship between rest length and moisture

⁴As observed by Grinspun et al [2006], the *shape operator* $d\hat{n}$ in the continuous setting always maps tangent vectors to tangent vectors, whereas in the discrete setting the finite difference of mid-edge normals is not always parallel to the mesh triangle. This discrepancy is a consequence of the failure of edge-offset meshes to also be face-offsets. Corrections to the shape operator have been proposed to remedy this quirk, though we found them unnecessary (and in any case, any components of $d\hat{n}$ that lie orthogonal to the face are annihilated when forming the second fundamental form $-dr^T d\hat{n}$).

concentration [?], the rest metric of the shell at the top and bottom of the thickness is given by

$$\bar{g}^+ = (1 + m^+ \mu)^2 (a^0 - hb^0), \quad \bar{g}^- = (1 + m^- \mu)^2 (a^0 + hb^0),$$

for an experimentally determined parameter μ relating moisture to length. Then

$$\bar{a} = \frac{(1 + m^+ \mu)^2 + (1 + m^- \mu)^2}{2} a^0 + h \frac{(1 + m^- \mu)^2 - (1 + m^+ \mu)^2}{2} b^0$$

$$\bar{b} = \frac{(1 + m^- \mu)^2 - (1 + m^+ \mu)^2}{2h} a^0 + \frac{(1 + m^+ \mu)^2 + (1 + m^- \mu)^2}{2} b^0.$$

- **Piecewise Constant Differential Swelling** Instead of a linear moisture gradient through the thickness, in some cases it is more appropriate to model a piecewise constant moisture profile, such as when modeling bilayers with different material properties. For example, XXX et al [?] fabricate exotic pasta geometries by cooking pasta composed of two layers of different porosity. van Reese et al [?] showed that a bilayer of thickness h with piecewise-constant rest metric

$$\bar{g}(z) = \begin{cases} \bar{g}^+, z > 0 \\ \bar{g}^-, z < 0 \end{cases}$$

is *energetically equivalent* to a shell with linearly-varying metric

$$\bar{a} = \frac{\bar{g}^+ + \bar{g}^-}{2}, \quad \bar{b} = \frac{3}{4h} (\bar{g}^- - \bar{g}^+);$$

thus the desired piecewise-constant metric taking into account moisture-induced swelling is

$$\bar{g}^+ = (1 + m^+ \mu^+)^2 \left(a^0 - \frac{2}{3} hb^0 \right), \quad \bar{g}^- = (1 + m^- \mu^-)^2 \left(a^0 + \frac{2}{3} hb^0 \right),$$

where μ^+ and μ^- encode the differing moisture-length relationship in the two layers. Converting this piecewise-constant metric back into the equivalent linear metric gives

$$\bar{a} = \frac{(1 + m^+ \mu^+)^2 + (1 + m^- \mu^-)^2}{2} a^0 + h \frac{(1 + m^- \mu^-)^2 - (1 + m^+ \mu^+)^2}{3} b^0$$

$$\bar{b} = 3 \frac{(1 + m^- \mu^-)^2 - (1 + m^+ \mu^+)^2}{4h} a^0 + \frac{(1 + m^+ \mu^+)^2 + (1 + m^- \mu^-)^2}{2} b^0.$$

- **Linear Differential Swelling with Machine Direction** In paper, leaves, and other materials composed of microscopic fibers, swelling induced by moisture is *anisotropic*, since fibers swell more in their circumferential than axial direction. We can model this behavior by storing a *machine direction* d_{ijk} per triangle face; this direction, a vector in the barycentric coordinates of the triangle, is the direction in which the fibers are aligned. Given this direction, we can compute the intrinsically orthogonal direction d_{ijk}^\perp (with $d_{ijk}^T d_{ijk}^\perp = 0$), and impose different moisture-length constants μ and μ_\perp in the d and d^\perp directions, respectively. Then the desired rest metrics at the top and bottom of the shell are

$$\bar{g}^+ = T^T M^+ T^{-T} (a^0 - hb^0) T^{-1} M^+ T,$$

$$\bar{g}^- = T^T M^- T^{-T} (a^0 + hb^0) T^{-1} M^- T.$$

where

$$T = [\mathbf{d} \quad \mathbf{d}_\perp]$$

transforms from the triangle's barycentric coordinates to the $\mathbf{d}, \mathbf{d}_\perp$ coordinate system, and

$$M^\pm = \begin{bmatrix} (1 + m^\pm \mu) & 0 \\ 0 & (1 + m^\pm \mu_\perp) \end{bmatrix}$$

anisotropically stretches in the machine direction. As in the previous cases, the rest fundamental forms can be computed from these metrics using the formula

$$\bar{\mathbf{a}} = \frac{\bar{\mathbf{g}}^+ + \bar{\mathbf{g}}^-}{2}, \quad \bar{\mathbf{b}} = \frac{\bar{\mathbf{g}}^- - \bar{\mathbf{g}}^+}{2h}.$$

Elastic Energy. We can now write down the full elastic energy of the shell, in exact analogy to the Koiter energy:

$$E_{\text{elastic}}(\mathbf{v}) = \sum_{f_{ijk} \in F} \frac{\sqrt{\det \bar{\mathbf{a}}_{ijk}}}{2} \left(\frac{h}{4} \|\bar{\mathbf{a}}_{ijk}^{-1} \mathbf{a}_{ijk} - I\|_{SV}^2 + \frac{h^3}{12} \|\bar{\mathbf{a}}_{ijk}^{-1} (\mathbf{b}_{ijk} - \bar{\mathbf{b}}_{ijk})\|_{SV}^2 \right)$$

It is worth making a few observations about this energy. First, the matrices \mathbf{a} , $\bar{\mathbf{a}}$, etc. are *coordinate-dependent*: replacing the parameterization domain \mathcal{T} , or even cyclically permuting the order of vertices around a face, would alter the values in the matrix. However, the generalized eigenvalues of $\mathbf{a} - \bar{\mathbf{a}}$ and $\mathbf{b} - \bar{\mathbf{b}}$ with respect to the inner product $\bar{\mathbf{a}}$ are *coordinate-independent*, as is the total energy. Perhaps the easiest way to see this fact is to note that these spectra measure the geometrically exact strain induced by an affine embedding of \mathcal{T} , and so *must* be independent of the coordinates chosen. Second, the terms of the form $\|\bar{\mathbf{a}}^{-1} M\|_{SV}^2$ are sometimes instead written as $\|\bar{\mathbf{a}}^{-1/2} M \bar{\mathbf{a}}^{-1/2}\|_{SV}^2$, where $\bar{\mathbf{a}}^{-1/2}$ is the unique positive-definite square root of $\bar{\mathbf{a}}$. The two expressions are equivalent, since the spectrum of a product of matrices is invariant under cyclic permutation, but the form used above is slightly more convenient for computation. Finally, as a sanity check, observe that when $\bar{\mathbf{b}} = 0$ and the Poisson ratio $\nu = 0$, the bending energy reduces to the square of mean curvature, as expected for thin plates.

Mass Matrix. As in the continuous formulation, the density ρ_{ijk} of each face might change over time due to absorption or evaporation of moisture. We use a piecewise-constant discretization of density

$$\rho_{ijk} = \rho_{\text{shell}} + \frac{m_{ijk}^+ + m_{ijk}^-}{2} \rho_{\text{water}},$$

where ρ_{shell} and ρ_{water} are the densities of the shell material and water, respectively, and construct a typical Galerkin mass matrix M for the midsurface vertices. (In simulations where shell deformation is driven by a mechanism other than moisture changes, we drop the second term and use a constant density.)

Viscous Damping. Since the growth and swelling phenomena we want to simulate all take place at relatively long time scales, and paper and plastic are viscoelastic, a damping model is needed to dissipate the elastic waves in the material. We implement a simple

Kelvin-Voigt damping model by including a damping potential

$$E_{\text{damp}}(\mathbf{v}, \mathbf{v}^{\text{prev}}) = \eta \Delta t \sum_{f_{ijk} \in F} \frac{\sqrt{\det \bar{\mathbf{a}}_{ijk}}}{2} \left(\frac{h}{4} \left\| \bar{\mathbf{a}}_{ijk}^{-1} \frac{\mathbf{a}_{ijk} - \mathbf{a}_{ijk}^{\text{prev}}}{\Delta t} \right\|_{SV}^2 + \frac{h^3}{12} \left\| \bar{\mathbf{a}}_{ijk}^{-1} \frac{\mathbf{b}_{ijk} - \mathbf{b}_{ijk}^{\text{prev}}}{\Delta t} \right\|_{SV}^2 \right)$$

where Δt is the time step size, \mathbf{v}^{prev} denotes the values of \mathbf{v} in the previous time step (and likewise for \mathbf{a}^{prev} , etc), and η is a viscosity parameter.

Summary. In the discrete simulation, we track the following variables:

- The configuration \mathbf{v} and configurational velocity $\dot{\mathbf{v}}$. These vertex positions completely encode the kinematics of the discrete shell.
- Two matrices $\bar{\mathbf{a}}$ and $\bar{\mathbf{b}}$ per face in F , both symmetric, and with $\bar{\mathbf{a}}$ positive-definite. These matrices store information about the rest state of the discrete shell, and may change over the course of the simulation. In most of our simulations, the mechanism for changes in the shell rest state is absorption or evaporation of moisture; in this case we store two scalars m^+ and m^- per face, indicating moisture concentration on the top and bottom boundary of the shell, and $\bar{\mathbf{a}}$ and $\bar{\mathbf{b}}$ are computed from these scalars, as described above.

In addition, we track a machine direction \mathbf{d} per face, which doesn't change over the course of the simulation; finally Table ?? lists the physical parameters and constants on which the simulation depends, as well as reasonable values of these parameters for the special case of ordinary paper. We use these default values in all experiments described below, unless specified otherwise.

Time Integration. We integrate the equations of motion using implicit Euler:

$$M \frac{\dot{\mathbf{v}}^{i+1} - \dot{\mathbf{v}}^i}{\Delta t} = \mathbf{F}_{\text{ext}}(\mathbf{v}^{i+1}) - \nabla E_{\text{elastic}}(\mathbf{v}^{i+1}) - \nabla E_{\text{damp}}(\mathbf{v}^{i+1}, \mathbf{v}^i) \\ \mathbf{v}^{i+1} = \mathbf{v}^i + \Delta t \dot{\mathbf{v}}^{i+1},$$

where superscripts denote the time step index and \mathbf{F}_{ext} encapsulates contact forces and external forces like gravity. Solving these equations requires computing first and second derivatives of the elastic energy; the derivatives of a triangle's stretching term depend only on the vertices of that triangle, whereas the derivatives of the bending term also depend on vertices of the neighboring three triangles (due to the dependence of \mathbf{b} on the mid-edge normals). The bending term in particular is somewhat unpleasant to differentiate due to its high degree of nonlinearity, and special cases that arise for triangles adjacent to the mesh boundary. We provide formulas for the derivatives in the Appendix, and source code for calculating the derivatives in the supplemental material.

4 MOISTURE DIFFUSION

5 RESULT

We evaluate the simulation on a variety of examples, both didactic and complex.

571 5.1 Analytic Benchmarks

572 We first test the method on examples where the equilibrium state
 573 can be computed exactly. When an embedding \mathbf{r} exists for which
 574 $\mathbf{a} = \bar{\mathbf{a}}$ and $\mathbf{b} = \bar{\mathbf{b}}$, that embedding is clearly a global minimizer of
 575 the elastic energy, regardless of material parameters. We ran all of
 576 the following experiments using the default values in Table ?? . We
 577 assigned a viscosity $\gamma = XXX$ to the material and ran the simulation
 578 for YYY seconds, enough time for the simulation to reach steady
 579 state.

580 *Uniform Swelling of Square.* We take Ω to be a unit square, with
 581 $\mathbf{r} = \text{id}$, and assign a constant $\bar{\mathbf{a}}$ and $\bar{\mathbf{b}}$ to the entire shell. Table 1
 582 summarizes the values of $\bar{\mathbf{a}}$ and $\bar{\mathbf{b}}$ we tried, and the expected shape
 583 and curvatures of the exact solution. We ran the simulation using
 584 a coarse, fine, and nonuniform mesh (XXX, YYY, and ZZZ vertices
 585 respectively); simulated and exact solutions are compared in Fig-
 586 ure ?? . For all experiments except the hyperboloid, we compute the
 587 Hausdorff error between the steady state simulation mesh and the
 588 analytic solution. The hyperboloid does not have a single equilib-
 589 rium state; the energy landscape is "sombrero-like" with a curve of
 590 possible solutions, corresponding to intrinsic rotation of the hyper-
 591 boloid. For this experiment we instead measure the sum of squared
 592 mean and Gauss curvature, where the mesh's curvatures were mea-
 593 sured using quadratic fitting [?].

594 *Isotropic Growth.* The Riemann mapping theorem guarantees that
 595 every surface M with disk topology can be parameterized by the unit
 596 disk, with metric conformally equivalent to the Euclidean metric.
 597 This insight was exploited by Kim et al [] to grow a sphere from a
 598 square. In the case that M is flat, and this conformal metric is $\mathbf{a} = e^{2s} I$
 599 for conformal factor s , then a disk with prescribed fundamental
 600 forms

$$\bar{\mathbf{a}} = e^{2s} I, \quad \bar{\mathbf{b}} = 0$$

601 is expected to grow into M (up to rigid motion), since M is a global
 602 minimizer of the elastic energy. We use this fact as a basis for a test:
 603 we conformally map a XXX to the unit disk using the method of
 604 Crane [], assign a rest metric $\bar{\mathbf{a}}$ per the above formula, and simulate
 605 the resulting growth of the shell. Figure ?? compares the initial shape
 606 to the simulation steady state.

607 When M is not flat, we do not expect the shell to grow exactly into
 608 the shape M , since embedding the shell as the shape M minimizes
 609 stretching energy while ignoring bending energy. Nevertheless, we
 610 expect the steady state geometry to closely resemble M , especially
 611 for small shell thickness h . Figure ?? shows the result of attempting
 612 to swell the unit disk into a sphere, using the rest fundamental forms
 613 from Kim et al [?],

$$\bar{\mathbf{a}} = XXX, \quad \bar{\mathbf{b}} = 0.$$

618 5.2 Comparisons to Experiments

619 *Radial Swelling of Disk.*

620 *Curling of Paper.*

623 5.3 Effects of Parameters

624 *Poisson's Ratio.*

625 *Thickness.*

Machine Direction.

5.4 Comparison to Jeong et al

5.5 Qualitative Experiments

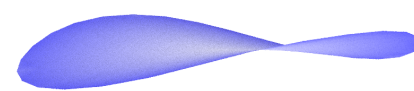
We end with several experiments that demonstrate the flexibility
 of the method to simulate complex geometry undergoing complex
 nonlinear deformations due to differential swelling.

The Walker.

The Caterpillar.

The Spoon.

6 OLD TEXT



641 **Hougaard**

642 (a) Caption 1



643 **Hougaard**

644 (b) Caption 2

6.0.1 Radially Wet Disc.

6.0.2 Machine Direction Experiment.

6.0.3 Dried Leaves.

6.0.4 Wetting Paper Annulus.

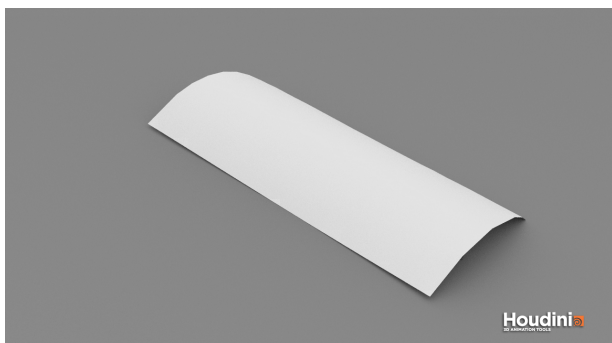
6.0.5 Wetting Straw Wrapping Paper.

6.0.6 Melting Spoon.

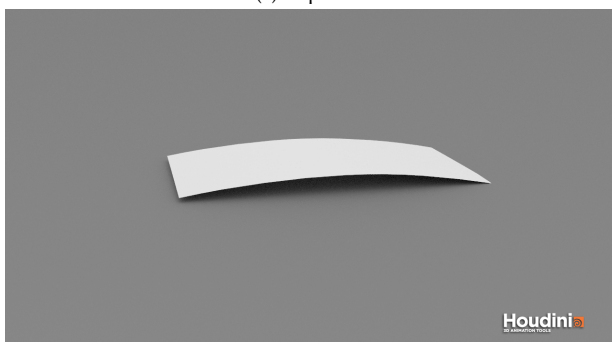
6.0.7 Melting Torus.

	\bar{a}	\bar{b}	Expected Shape	H	K	Error (coarse)	Error (fine)	Error (nonuniform)	
685	$2I$	0	Enlarged Square	0	0	XXX	XXX	XXX	742
686	I	I	Spherical Cap	2	1	XXX	XXX	XXX	743
687	I	$-I$	Hyperboloid Cap	-2	-1	XXX	XXX	XXX	744
688	$\begin{pmatrix} 2 & 1 \\ 1 & 2 \end{pmatrix}$	0	Rhombus	0	0	XXX	XXX	XXX	745
689	I	$\begin{pmatrix} 1 & 0 \\ 0 & 0 \end{pmatrix}$	Cylindrical Patch	1	0	XXX	XXX	XXX	746
690									747
691									748
692									749

Table 1. Didactic experiments on a unit square. Different \bar{a} and \bar{b} are prescribed uniformly over the square, and in each case we compare the simulated steady state to the expected analytic solution.



(a) Caption1



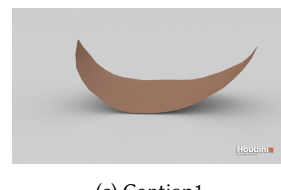
(b) Caption 2



(a) Caption1



(b) Caption 2



(c) Caption1



(d) Caption 2

Fig. 3. Simulation for Dried Leaves

7 CONCLUSIONS AND FUTURE WORK

REFERENCES

- Kosala Bandara and Fehmi Cirak. 2018. Isogeometric shape optimisation of shell structures using multiresolution subdivision surfaces. *Computer-Aided Design* 95, Supplement C (2018), 62 – 71. <https://doi.org/10.1016/j.cad.2017.09.006>
- David Baraff and Andrew Witkin. 1998. Large Steps in Cloth Simulation. In *Proceedings of the 25th Annual Conference on Computer Graphics and Interactive Techniques (SIGGRAPH '98)*. ACM, New York, NY, USA, 43–54. <https://doi.org/10.1145/280814.280821>
- Klaus JÄJrgen Bathe, Eduardo Dvorkin, and Lee W. Ho. 1983. Our discrete-Kirchhoff and isoparametric shell elements for nonlinear analysis—An assessment. *Computers & Structures* 16, 1 (1983), 89 – 98. [https://doi.org/10.1016/0045-7949\(83\)90150-5](https://doi.org/10.1016/0045-7949(83)90150-5)
- Jean-Louis Batoz, Klaus-JÄJrgen Bathe, and Lee-Wing Ho. 1980. A study of three-node triangular plate bending elements. *Internat. J. Numer. Methods Engrg.* 15, 12 (1980), 1771–1812. <https://doi.org/10.1002/nme.1620151205>
- D.J. Benson, Y. Bazilevs, M.C. Hsu, and T.J.R. Hughes. 2010. Isogeometric shell analysis: The Reissner-Mindlin shell. *Computer Methods in Applied Mechanics and Engineering* 199, 5 (2010), 276 – 289. <https://doi.org/10.1016/j.cma.2009.05.011> Computational Geometry and Analysis.
- Miklos Bergou, Max Wardetzky, David Harmon, Denis Zorin, and Eitan Grinspun. 2006. A Quadratic Bending Model for Inextensible Surfaces. In *Proceedings of the Fourth Eurographics Symposium on Geometry Processing (SGP '06)*. Eurographics Association, Aire-la-Ville, Switzerland, Switzerland, 227–230.
- Alexander I. Bobenko, Helmut Pottmann, and Johannes Wallner. 2010. A curvature theory for discrete surfaces based on mesh parallelity. *Math. Ann.* 348, 1 (01 Sep 2010), 1–24. <https://doi.org/10.1007/s00208-009-0467-9>
- Alexander I. Bobenko and Peter Schröder. 2005. Discrete Willmore Flow. In *Proceedings of the Third Eurographics Symposium on Geometry Processing (SGP '05)*. Eurographics Association, Aire-la-Ville, Switzerland, Switzerland, Article 101.

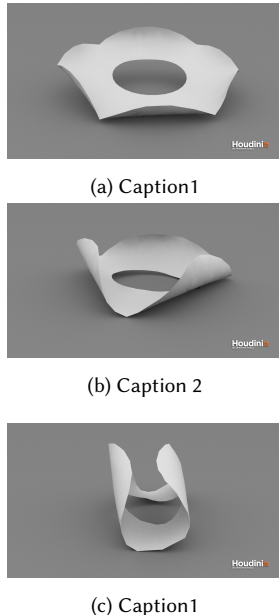


Fig. 4. Simulation for Wet Annulus

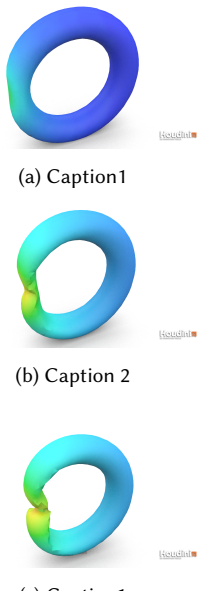


Fig. 5. Simulation for Dried Torus

- Robert Bridson, Ronald Fedkiw, and John Anderson. 2002. Robust Treatment of Collisions, Contact and Friction for Cloth Animation. *ACM Trans. Graph.* 21, 3 (July 2002), 594–603. <https://doi.org/10.1145/566654.566623>
- Philippe G. Ciarlet. 2000. *Theory of Shells, Volume 3 (Mathematical Elasticity)*. North Holland.
- Fehmi Cirak, Michael Ortiz, and Peter Schröder. 2000. Subdivision surfaces: a new paradigm for thin-shell finite-element analysis. *Internat. J. Numer. Methods Engrg.* 47, 12 (2000), 2039–2072. [https://doi.org/10.1002/\(SICI\)1097-0207\(20000430\)47:12<2039::AID-NME872>3.0.CO;2-1](https://doi.org/10.1002/(SICI)1097-0207(20000430)47:12<2039::AID-NME872>3.0.CO;2-1)

- E. Efrati, E. Sharon, and R. Kupferman. 2009. Elastic theory of unconstrained non-Euclidean plates. *Journal of the Mechanics and Physics of Solids* 57, 4 (2009), 762 – 775. <https://doi.org/10.1016/j.jmps.2008.12.004> 856
857
- Eitan Grinspun, Yotam Gingold, Jason Reisman, and Denis Zorin. 2006. Computing discrete shape operators on general meshes. *Computer Graphics Forum* 25, 3 (2006), 547–556. <https://doi.org/10.1111/j.1467-8659.2006.00974.x> 858
859
- Eitan Grinspun, Anil N. Hirani, Mathieu Desbrun, and Peter Schröder. 2003. Discrete Shells. In *Proceedings of the 2003 ACM SIGGRAPH/Eurographics Symposium on Computer Animation (SCA '03)*. Eurographics Association, Aire-la-Ville, Switzerland, Switzerland, 62–67. 860
861
- SoHyeon Jeong, Tae-hyeong Kim, and Chang-Hun Kim. 2011. Shrinkage, Wrinkling and Ablation of Burning Cloth and Paper. *Vis. Comput.* 27, 6–8 (June 2011), 417–427. <https://doi.org/10.1007/s00371-011-0575-x> 863
864
- SoHyeon Jeong, Si-Hyung Park, and Chang-Hun Kim. 2013. Simulation of Morphology Changes in Drying Leaves. *Computer Graphics Forum* 32, 1 (2013), 204–215. <https://doi.org/10.1111/cgf.12009> 866
867
- J. Kiendl, K.-U. Bletzinger, J. Linhard, and R. Wüchner. 2009. Isogeometric shell analysis with Kirchhoff-Love elements. *Computer Methods in Applied Mechanics and Engineering* 198, 49 (2009), 3902 – 3914. <https://doi.org/10.1016/j.cma.2009.08.013> 868
869
- J. Kim, J.A. Hanna, M. Byun, C.D. Santangelo, and R.C. Hayward. 2012. Designing responsive buckled surfaces by halftone gel lithography. *Science* 335, 6073 (2012), 1201–1205. 870
871
- Yael Klein, Efi Efrati, and Eran Sharon. 2007. Shaping of Elastic Sheets by Prescription of Non-Euclidean Metrics. *Science* 315, 5815 (2007), 1116–1120. <https://doi.org/10.1126/science.1135994> arXiv:<http://science.sciencemag.org/content/315/5815/1116.full.pdf> 872
873
- Caroline Larboulette, Pablo Quesada, and Olivier Dumas. 2013. Burning Paper: Simulation at the Fiber's Level. In *Proceedings of Motion on Games (MIG '13)*. ACM, New York, NY, USA, Article 25, 6 pages. <https://doi.org/10.1145/2522628.2522906> 874
875
- Shiguang Liu, Qiguang Liu, Tai An, Jizhou Sun, and Qunsheng Peng. 2009. Physically based simulation of thin-shell objects' burning. *The Visual Computer* 25, 5 (01 May 2009), 687–696. <https://doi.org/10.1007/s00371-009-0344-2> 877
878
- Frank Losasso, Geoffrey Irving, Eran Guendelman, and Ron Fedkiw. 2006. Melting and Burning Solids into Liquids and Gases. *IEEE Transactions on Visualization and Computer Graphics* 12, 3 (May 2006), 343–352. <https://doi.org/10.1109/TVCG.2006.51> 879
880
- Zeki Melek and John Keyser. 2003. Interactive Simulation of Burning Objects. In *Proceedings of the 11th Pacific Conference on Computer Graphics and Applications (PG '03)*. IEEE Computer Society, Washington, DC, USA, 462–. 881
882
- Zeki Melek and John Keyser. 2005. Multi-representation Interaction for Physically Based Modeling. In *Proceedings of the 2005 ACM Symposium on Solid and Physical Modeling (SPM '05)*. ACM, New York, NY, USA, 187–196. <https://doi.org/10.1145/1060244.1060265> 883
884
- Zeki Melek and John Keyser. 2007. Driving Object Deformations from Internal Physical Processes. In *Proceedings of the 2007 ACM Symposium on Solid and Physical Modeling (SPM '07)*. ACM, New York, NY, USA, 51–59. <https://doi.org/10.1145/1236246.1236257> 885
886
- Rahul Narain, Armin Samii, and James F. O'Brien. 2012. Adaptive Anisotropic Remeshing for Cloth Simulation. *ACM Trans. Graph.* 31, 6, Article 152 (Nov. 2012), 10 pages. <https://doi.org/10.1145/2366145.2366171> 887
888
- P. Neff. 2004. A geometrically exact Cosserat shell-model including size effects, avoiding degeneracy in the thin shell limit. Part I: Formal dimensional reduction for elastic plates and existence of minimizers for positive Cosserat couple modulus. *Continuum Mechanics and Thermodynamics* 16, 6 (01 Oct 2004), 577–628. <https://doi.org/10.1007/s00161-004-0182-4> 889
890
- Eran Sharon and Efi Efrati. 2010. The mechanics of non-Euclidean plates. *Soft Matter* 6 (2010), 5693–5704. Issue 22. <https://doi.org/10.1039/C0SM00479K> 891
892
- J.C. Simo and D.D. Fox. 1989. On a stress resultant geometrically exact shell model. Part I: Formulation and optimal parametrization. *Computer Methods in Applied Mechanics and Engineering* 72, 3 (1989), 267 – 304. [https://doi.org/10.1016/0045-7825\(89\)90002-9](https://doi.org/10.1016/0045-7825(89)90002-9) 893
894
- John M. Sullivan. 2008. *Curvatures of Smooth and Discrete Surfaces*. Birkhäuser Basel, Basel, 175–188. https://doi.org/10.1007/978-3-7643-8621-4_9 895
896
- Rasmus Tamstorf and Eitan Grinspun. 2013. Discrete bending forces and their Jacobians. *Graphical Models* 75, 6 (2013), 362 – 370. <https://doi.org/10.1016/j.gmod.2013.07.001> 897
898
- Roman Vetter, Norbert Stoop, Thomas Jenni, Falk K. Wittel, and Hans-Jürgen Zimmermann. 2013. Subdivision shell elements with anisotropic growth. *Internat. J. Numer. Methods Engrg.* 95, 9 (2013), 791–810. <https://doi.org/10.1002/nme.4536> 899
900
- Max Wardetzky, Miklós Bergou, David Harmon, Denis Zorin, and Eitan Grinspun. 2007. Discrete Quadratic Curvature Energies. *Comput. Aided Geom. Des.* 24, 8–9 (Nov. 2007), 499–518. <https://doi.org/10.1016/j.cagd.2007.07.006> 901
902
- Anna Wawrzinek, Klaus Hildebrandt, and Konrad Polthier. 2011. Koiter's Thin Shells on Catmull-Clark Limit Surfaces. In *Vision, Modeling, and Visualization (2011)*, Peter Eisert, Joachim Hornegger, and Konrad Polthier (Eds.). The Eurographics Association. <https://doi.org/10.2312/PE/VMV/VMV11/113-120> 903
904
- Clarisse Weischedel. 2012. *A discrete geometric view on shear-deformable shell models*. Ph.D. Dissertation. Georg-August-Universität Göttingen. 905
906
- , Vol. 1, No. 1, Article . Publication date: December 2018. 907
908
- 2017-12-02 14:42 page 8 (pp. 1-8) 909
910